Simple approach for modeling unidirectionally arrayed chopped strand laminates via the extended finite-element method

Yashiro, Shigeki
Department of Aeronautics and Astronautics, Kyushu University

Okuda, Tatsuya
Department of Aeronautics and Astronautics, Kyushu University

Ogi, Keiji
Graduate School of Science and Engineering, Ehime University

Nishikawa, Masaaki
Department of Mechanical Engineering and Science, Kyoto University

他

出版情報：Composite Structures. 229, pp.111457-, 2019-12-01. Elsevier
バージョン：
権利関係：

Composite Structures 229 (2019) 111457
DOI: 10.1016/j.compstruct.2019.111457

Simple approach for modeling unidirectionally arrayed chopped strand laminates via the extended finite-element method

Shigeki Yashiro [1,*], Tatsuya Okuda [1], Keiji Ogi [2], Masaaki Nishikawa [3], Hiroto Nagai [1]

[1] Department of Aeronautics and Astronautics, Kyushu University

744 Motooka, Nishi-ku, Fukuoka 819-0395, Japan

[2] Graduate School of Science and Engineering, Ehime University

3 Bunkyo-cho, Matsuyama, Ehime 790-8577, Japan

[3] Department of Mechanical Engineering and Science, Kyoto University

Building C3, Nishikyo-ku, Kyoto 615-8540, Japan

* Corresponding author: yashiro@aero.kyushu-u.ac.jp (S. Yashiro)

Abstract

This study presents a simple approach to model unidirectionally arrayed chopped strand (UACS) laminates via the extended finite-element method to represent slits (i.e., fiber cutting lines). This enables the introduction of slits independent of the finite-element mesh and reduces the effort to represent a complex discontinuity pattern when compared to standard modeling using double nodes. The laminated structure was represented by stacking two-dimensional

layers, and cohesive elements were inserted into the layer interfaces to predict the extension of delamination. Damage progress in CFRP quasi-isotropic laminates with diagonal continuous slits were analyzed via the present approach, and the effect of the angle between the slit line and fiber direction on the tensile strength was investigated. The predicted strength was in agreement with the reported experiment results within the examined slit angle range. A numerical study revealed that the strength of the UACS laminates was enhanced by a low inclined slit angle.

Keywords: Polymer-matrix composites (PMCs); Platelet structure; Extended finite-element method (XFEM); Delamination

1. Introduction

Carbon-fiber-reinforced plastics (CFRPs) are widely used in airplanes and general products due to their high specific strength and stiffness. Additionally, CFRPs are also promising for automobiles in terms of reducing structural weight and improving fuel consumption efficiency. Structural components of automobiles and general machines exhibit complex geometries. Therefore, formability is important for the material in addition to strength and stiffness. In the past years, components with a complex shape were manufactured via injection molding and

sheet molding compound (SMC) press molding. Good formability is achieved by the molding methods given the flow of discontinuous fibers. However, polymer-matrix composites reinforced by discontinuous fibers generally exhibit poor strength properties [1] because it is not possible to control the microstructure in the molding process. Conversely, stacking prepreg sheets with continuous fibers provide regular microstructure albeit poor flowability via press molding. High mechanical properties and good formability of CFRPs are not realized simultaneously, and thus CFRPs have not yet replaced metals in complex-shaped components. Research and development are being conducted to tackle these issues [2,3].

In order to overcome the trade-off relationship between strength and formability, Taketa et al. [4] proposed unidirectionally arrayed chopped strands (UACS) in which unidirectional fibers of prepreg sheets are cut in a regular manner (Fig. 1a). Specifically, UACS is an assembly of several sheets similar to the SMCs. However, the high structural regularity is the key difference between the UACS and SMCs. Given the regular arrangement of sheets, UACS exhibit stiffness close to that of continuous CFRPs, strength significantly exceeding that of SMCs, and good formability comparable to SMCs.

A few properties of laminates fabricated using UACS are investigated. Taketa et al. [4] indicated that the strength of unidirectional UACS laminates made of general-purpose

carbon/epoxy prepreg sheets is governed by unstable growth of delamination and presented a simple theoretical model to predict their tensile strength. Taketa et al. improved the strength of UACS laminates via toughening ply interfaces [5] and changing the pattern of fiber cuttings (called slits) [6]. In the case of diagonal continuous slits (Fig. 1b), the effect of the angle between the fiber direction and slits (hereafter referred to as the slit angle) on the tensile strength was examined, and a lower slit angle increased the strength. Furthermore, various strength properties [7] and flowability in press molding [8] were also investigated. Li et al. [9] examined the strength and flowability of UACS laminates with diagonal discontinuous slits. Strength was enhanced via designing new slit patterns. The results indicated that the UACS laminate with discontinuous bi-angled slits exhibited the highest flowability and uniformity. Sudarsono and Ogi [10,11] performed fatigue tests of open-holed UACS laminates with diagonal discontinuous slits and observed the effect of the slit angle on the damage extension and fatigue properties. Li et al. [12] predicted tensile damage progress in UACS laminates with diagonal discontinuous slits via a finite-element model that explicitly represented the slit structure. The homogenization method was employed to predict the effective elastic constants of the middle UACS plies to decrease computation costs. Kravchenko et al. [13,14] developed a representative volume element of regularly-arrayed platelet-based composite and investigated the effect of the meso-

structure on the macroscopic failure. The length-to-thickness ratio of a strand (platelet) is indicated to be a key parameter that governs the failure pattern.

Experimental studies demonstrated that both static strengths [6] and fatigue properties [11] were improved via a low slit angle. However, the mechanism of strength enhancement is unclear. Furthermore, evaluation of the strength of UACS laminates is essential to optimize the slit layout. Therefore, numerical modeling is important to achieve a better understanding and higher performance of the laminates. Slits (i.e., discontinuity of fibers) are represented by double nodes in the finite-element method in a manner similar to numerical studies [12,15]. However, extensive efforts are required for the preprocess via the standard approach because every change in the slit layout results in the re-development of a complex mesh with double nodes along the slits in all the plies. This acts as a severe obstacle in analyzing various properties of UACS laminates for optimizing the slit layout.

The extended finite-element method (XFEM) [16,17] represents the discontinuity of the displacement field due to a crack independent of the FE mesh, and it was recently applied to crack extension simulations [18]. Therefore, the present study employs XFEM to represent discontinuity in the displacement field produced by slits. The proposed approach significantly reduces the effort involved in the cumbersome preprocess for any slit layouts when compared

to that of the standard modeling method given the advantages of the XFEM.

This study presents modeling and damage extension analysis of UACS quasi-isotropic laminates with diagonal continuous slits. Specifically, the laminated structure is analyzed via the layer-wise method [15,19] with cohesive elements for adhesion and delamination of the ply interfaces, and slits are represented via the XFEM. The objective of this study is not to develop a new analysis 'method' but to present a new 'model' that requires less effort of preprocess for the specific meso-structure. To the authors' knowledge, there is no study that represents the regularly arrayed platelets using the XFEM and the layer-wise model. The static tensile strength of UACS laminates is evaluated and compared to the experimental results [6] to confirm the validity of the proposed approach. Furthermore, the effect of the slit angle on the tensile strength is discussed.

2. Analysis

2.1 Layer-wise finite element model

A laminate is separated into finite element layers that represent every ply of the stacking sequence, and two-dimensional solid elements or plate elements are used for these layers. The layer-wise model enables in analyzing the deformation of each ply and decreasing calculation

cost when compared to that of the three-dimensional model.

Adhesion and extension of delamination are analyzed via cohesive elements that are inserted into layer interfaces. This study used the following relationship between the traction T_i and separation Δ_i [20].

$$T_i = \frac{s}{1-s}\frac{\Delta_i}{\Delta_{ic}}\tau_{i\max} \ (i = n,t,b) \tag{1}$$

$$\Delta_{nc} = \frac{2G_{\mathrm{I}c}}{\tau_{n\max}s_{ini}}, \quad \Delta_{tc} = \frac{2G_{\mathrm{II}c}}{\tau_{t\max}s_{ini}}, \quad \Delta_{bc} = \frac{2G_{\mathrm{III}c}}{\tau_{b\max}s_{ini}} \tag{2}$$

Here, $\tau_{i\max}$ and Δ_{ic} (i = n, t, b) denote the maximum stress and critical relative displacement, respectively, at which the cohesive element cannot generate any traction; the subscripts n, t, and b denote the cracking modes of normal tension, in-plane shear, and out-of-plane shear, respectively, and G_{ic} (i = I, II, III) denotes the critical energy release rate. The parameter s determines the stiffness of a cohesive element, and its initial value is slightly less than unity. The parameter s is updated as a function of the normalized relative displacement vector $\tilde{\boldsymbol{\Delta}} = \left\{\Delta_n/\Delta_{nc}, \Delta_t/\Delta_{tc}, \Delta_b/\Delta_{bc}\right\}^T$ as follows:

$$s = \min\left(s_{\min}, \max\left(1 - \left|\tilde{\boldsymbol{\Delta}}\right|\right)\right) \tag{3}$$

The above cohesive element acts as a penalty element that imposes continuity of displacement field at the layer interface when s corresponds to the initial value. The parameter s decreases with increases in the relative displacement, and the cohesive element becomes a

crack without generating any traction force when s corresponds to zero. The cohesive element dissipates the energy equivalent to the critical energy release rate in its softening stage.

2.2 Extended finite-element method (XFEM)

This study employs the XFEM to represent the slits introduced into each ply independently of the FE mesh. Discontinuity in the displacement field and singularity of the stress field due to a crack are analyzed via enriching the interpolation function of the standard FEM with special functions. Displacement field at position $\mathbf{x}$ of an element near a crack, $\mathbf{u}^h$, is approximated as follows [16,17]:

$$\mathbf{u}^h(\mathbf{x}) = \sum_{I=1}^{m} \phi_I(\mathbf{x})\mathbf{U}_I + \sum_{I\in C} \phi_I(\mathbf{x}) \sum_{k=1}^{4} \gamma_k(\mathbf{x})\mathbf{a}_I^k + \sum_{I\in J} \phi_I(\mathbf{x}) H(\mathbf{x})\mathbf{b}_I \,, \tag{4}$$

where ϕ_I denotes the shape function of the standard FEM; m denotes the number of nodes in an element; and $\mathbf{U}_I$, $\mathbf{a}^k_I$, and $\mathbf{b}_I$ denote the degree of freedom of a node. Additionally, C denotes a set of nodes that considers the characteristics of the asymptotic solution near a crack tip, and J denotes a set of nodes that considers discontinuity of the displacement field by a crack. Furthermore, γ_k (k = 1, …, 4) denotes the basis function that represents the asymptotic solution of the displacement field near the crack tip, and $H(\mathbf{x})$ denotes the Heaviside function.

$$H(x) = \begin{cases} 1 & (x \geq 0) \\ -1 & (x < 0) \end{cases} \tag{5}$$

This study assumes that $H(x)$ corresponds to 1 on the upper side of the crack line and -1 on the lower side.

There was no *C*-type node in the model since all slits were continuous in this study. All nodes near slits were set to be *J*-type, and the third term of the right-hand-side of Eq. (4) was considered to represent the displacement field.

3. Tension analysis of UACS quasi-isotropic laminates

3.1 Analytical model

This study developed an in-house code for easily representing the meso-structure of UACS laminates. The analytical solution to predict the tensile strength of a UACS laminate agreed well with the experiment results [4]. The fracture toughness estimated from the measured tensile strength and a one-dimensional model coincided with the mode II interlaminar fracture toughness of CFRP laminates with the same resin system, which was measured via the interlaminar toughness tests [21-23]. Moreover, the hackle pattern, which is generated by interlaminar shearing, is clearly observed on the delaminated surfaces of the UACS laminates in supplementary experiments (Fig. 2). These results suggested that the interlaminar shear displacement was dominant for delamination growth and that contribution of mode I was

negligible. Therefore, in order to ensure the simplicity of the analysis, two-dimensional plane-stress elements were used to represent the layers. Strictly speaking, delamination grows under a mixed-mode condition, but only limited out-of-plane deformation is acceptable except at the ends of a plate. Therefore, we assumed that the shear mode is dominant in the delamination growth in a UACS laminate, and the out-of-plane displacement was omitted in the present model.

Figure 3 shows a schematic of the layer-wise finite-element model. The stacking sequence of the UACS laminates used in the reported experiment [6] was quasi-isotropic $[45/0/-45/90]_{2S}$, and four layers corresponding to 45°, 0°, -45°, and 90° were prepared and adhered via cohesive elements. In addition to the layer interfaces of 45°/0°, 0°/-45°, and -45°/90°, the top 90° layer and the bottom 45° layer were also coupled via a cohesive element. The model exhibited a periodic structure in the through-thickness direction to remove the effect of free surfaces on damage extension. In a manner similar to an experiment in an extant study [6], the model was 150 mm long and 25 mm wide, and the thickness of a layer was 0.14 mm. Four-node solid (plane-stress) elements were used, and all elements exhibited a square shape with 0.5 mm on a side. There were 61404 nodes and 60000 solid elements. Nine integral points were prepared for a numerical integral since the enriched function was included in the shape function in the XFEM.

Slits were represented by the XFEM. Figure 4 shows a set of *J*-type nodes for a slit angle of 27°. The distance between two adjacent slits (which corresponds to the fiber length) was 25 mm. Models with five slit angles (i.e., 16°, 27°, 45°, 60°, and 90°) were prepared, and the effect of the slit angle θ on the damage extension and tensile strength was investigated. Arrangement of *J*-type nodes at the initial condition corresponded to the approximation that the slits were cracks before loading although the actual slits were embedded by the matrix resin flow into the thin spaces of the fiber cuttings. It was noted that the slits became cracks by small deformation [15].

The left edge of the model (Fig. 3) was fixed in the longitudinal (x) direction, and uniform tensile displacement in the x-direction was applied to the right edge. Uniform displacement increment corresponding to 0.01% tensile strain was applied, and the displacement field was converged via the direct iteration method [24]. The applied stress was calculated as the sum of the nodal force of the right edge of the model divided by the cross-sectional area. Table 1 lists the material properties used. A general-purpose CFRP (T700S/#2500) was used in the experiment [6], and the interlaminar fracture toughness estimated for the same material [4] was employed. It should be noted that the out-of-plane displacement, as well as the crack opening mode in a cohesive element, is not taken into consideration because of the use of two-

dimensional elements. Two analyses were performed in advance to identify the effect of the element size; one is the result in the following section and the other employed the element size of 1 mm on a side (i.e., twice of the present model). The results were almost the same. Instead, the spacing between a discontinuity line and an integral point greatly affected the results. When an integral point was too close to a discontinuity line, the analysis could not reach convergence.

Experimental studies [4,6] revealed that the delamination (and not the fiber breaks) causes the final failure of the UACS laminates in most cases. In the present approach, delamination is analyzed via the cohesive elements at the layer interfaces, and the slits modeled by the XFEM corresponds to the source of its onset. It is noted that crack growth is not predicted by the XFEM in the analysis.

3.2 Analytical results and discussion

Figure 5 presents the predicted stress–strain curves. The applied stress linearly increased with increases in the strain up to 0.4% independent of the slit angle. The initial stiffness was in the range of 49.3 to 49.4 GPa, and this almost coincided with the Young's modulus calculated via the classical lamination theory without considering slits (49.5 GPa). The coincidence indicated that the spacing of slits was sufficiently large for stress recovery. When the applied strain

increased, stiffness gradually decreased due to softening of cohesive elements at the layer interfaces. The strain at a steep drop in stress varied with respect to the slit angle, and the maximum stress then depended on the slit angle. Figure 6 presents the relationship between the predicted maximum stress and slit angle θ along with the experiment results [6], in which supplementary experiment data is also plotted. The maximum stress increased with decreases in the θ within the range $\theta \leq 45°$. Otherwise, it was almost constant. The trend agreed with the experiment results. Furthermore, the prediction almost coincided with the experiment at slit angles over 45° at which the UACS laminates were broken via delamination in the experiment. The results demonstrated the validity of the present approach. The fact that the predicted maximum stress was lower than the experimental data at low slit angles suggests occurrence of the other type of damage (i.e., fiber breakage) in addition to delamination, and the mixed mode fracture is investigated in a future study.

Figure 7 depicts the delamination growth of the model with the slit angle of 16°. Softening of the cohesive elements first appeared at the layer interfaces adjacent to the 0° layer. Specifically, damage was accumulated near the intersections of slits in the 0° layer and in its adjacent layers. However, delamination barely extended even with increases in the applied strain. Delamination rapidly extended over 0.85% applied strain, and the stress decreased. In a

manner similar to the case of the slit angle of 16°, delamination extended at the 45°/0° and 0°/-45° interfaces in all the slit angles, and the other two interfaces were almost intact until the maximum stress was reached.

Figure 8 shows the damage state of the 0°/-45° interface at the maximum stress and after reaching the maximum stress in all the slit angles. Cohesive elements were softened along the slits of the 0° layer in all the slit angles. Slits in the 0° layer were likely to open given a high tensile stress, and this increased the relative displacement to the adjacent layer near the slits. Therefore, delamination initially appeared along the slits of the 0° layer. In low slit angles (Figs. 7a and 7b), delamination was generated only in small regions near the free edges until the maximum stress was reached. Shortly thereafter, delamination extended in the region surrounded by the slits in the 0° and -45° layers within a small strain increment. In contrast to the aforementioned cases, no area was surrounded by slits in large slit angles (Figs. 8c-8e). In these cases, delamination appeared near the free edges in the width direction prior to reaching the maximum stress and gradually extended along the slits of the 0° layer when the applied strain increased. The observation indicated that the mechanism of delamination growth affected the maximum tensile stress.

Thus, the present approach predicted the maximum stress of the quasi-isotropic UACS

laminates and generation of delamination at a load near the maximum stress. However, it is necessary to consider the out-of-plane deformation to predicting the whole fracture process (e.g., stable or unstable delamination growth), and this will be explored in a future study.

4. Effect of the slit angle on the strength

This section verifies the high strength of a UACS laminate at a low slit angle as shown in Fig. 6. Damage extension was analyzed in unidirectional laminates introducing slits with a constant inclined angle θ wherein the intersection of slits in adjacent layers is absent. It should be noted that unidirectional stacking in the present section is just a constituent of a quasi-isotropic laminate to investigate the impact of the slit angle on the strength and that the following predictions are not always the actual strength of UACS unidirectional laminates.

A two-layer model was prepared. Figure 9a depicts two types of the slit layout. The interval of two slits was 25 mm in the longitudinal direction, and the slit layout B is created by shifting the layout A to 12.5 mm in the longitudinal direction. The effect of the slit angle on the tensile strength was investigated, and the slit angles corresponded to 16°, 27°, 45°, 60°, and 90°. The model exhibits a length of 200 mm and width of ($25 \times 2 \tan\theta$) mm to match the position of slits along the two edges for the periodic boundary condition as shown in Fig. 9b. The width for $\theta =$

90° was 50 mm. The number of nodes and elements depended on the slit angle, and for example, there were 64000 nodes and 64962 elements in the model for θ = 16°. Periodic boundary conditions were applied to the free surfaces and free edges to eliminate the aforementioned effects on damage extension. Periodic stacking in the through-thickness direction was created by connecting the surface two layers using cohesive elements as in the previous section. Periodic structure in the transverse direction was realized by conforming the displacement distribution of the edges to that along the centerline via the penalty method. Material properties listed in Table 1 are used with the exception of the fracture toughness, and G_{IIc} and G_{IIIc} are 1000 J/m^2.

Figure 10 shows the predicted stress–strain curves. Stiffness decreased gradually with increases in the applied strain, and the result suggested stable delamination growth. Figure 11 presents the relationship between the predicted maximum stress and slit angle θ. The maximum stress increased with decreases in the θ within the range $\theta \leq 45°$. Otherwise, it was almost constant. The tendency coincided with the results of quasi-isotropic laminates (Fig. 6). We consider the *x'*-*y'* coordinate shown in Fig. 12 where the *x'*-direction is along a slit. Stress components $\sigma_{y'}$ and $\tau_{x'y'}$ induced mode I opening and mode II shearing near the slit, respectively, and both modes generated relative displacement between the adjacent layers. When the uniaxial

stress σ_{app} is loaded in the x-direction, then $\sigma_{y'}$ and $\tau_{x'y'}$ acting on an element are calculated as a function of the slit angle θ as follows:

$$\sigma_{y'} = \sigma_{app} \sin^2 \theta \tag{6}$$

$$\tau_{x'y'} = -\frac{1}{2} \sigma_{app} \sin 2\theta \tag{7}$$

where $\sigma_{y'}$ and absolute value of $\tau_{x'y'}$ increase with increases in the θ within the range $\theta \leq 45°$. The stresses lead to a greater difference in the displacement field of the two layers near the slits with a larger slit angle. Figure 13 shows distribution of the relative displacement in the x'-y' coordinate system at the applied strain of 0.5% for θ = 16° and 45°. Jagged peaks appeared given the irregular distance from a slit to a displayed point. The maximum $\Delta_{x'}$ was almost the same. However, $\Delta_{y'}$ for θ = 16° was significantly lower than that for θ = 45°. The result suggested that delamination is less likely to occur with a lower slit angle and that the tensile strength increased with decreases in the θ within a low slit angle range. Within the range $\theta \geq$ 45°, the absolute value of $\tau_{x'y'}$ decreased although $\sigma_{y'}$ increased monotonically with increases in θ. Thus, the maximum stress was almost constant relative to the slit angle.

5. Conclusions

This study proposed a simple approach for modeling UACS laminates with slits (i.e., discontinuity lines of fibers) in each ply. Finite-element layers were prepared corresponding to

the stacking sequence, and cohesive elements were inserted into the layer interfaces to represent adhesion and delamination. Furthermore, the use of the XFEM enabled in analyzing the discontinuity of the displacement field by slits independently of the finite-element mesh. Given the absence of laborious mesh division along the slits, the present approach requires less effort to develop a model of a UACS laminate when compared to the standard model using double nodes. In the model, delamination growth was analyzed via the cohesive elements, and the slits represented by the XFEM corresponded to a source of onset of delamination.

This study predicted damage growth in a quasi-isotropic UACS laminate with diagonal continuous slits subjected to tensile loading. Changes in the tensile strength due to the slit angle were in agreement with the reported experiment results [6] within the range of the slit angle at which delamination dominates the final failure. Delamination was likely to be generated independent of the slit angle at the interfaces adjacent to the 0° layer due to high stress in the 0° ply. At low slit angles, small delamination initially appeared near the free edges and subsequently extended in the region surrounded by the slits of the upper and lower layers. At slit angles exceeding 45°, delamination was generated near the free edges at a small applied strain and extended gradually. A parametric study for unidirectional UACS laminates indicated that the mode I opening of slits was suppressed by a low slit angle and that the tensile strength

of UACS laminates was enhanced by a reduced slit angle given the decreased likelihood of the onset of delamination.

References

[1] Thomason JL. The influence of fibre length and concentration on the properties of glass fibre reinforced polypropylene: 5. Injection moulded long and short fibre PP. Compos Part A 2002; 33:1641–1652.

[2] Hashimoto M, Okabe T, Nishikawa M. Development of thermoplastic press sheet with in-plane randomly oriented and dispersed carbon mono-fibers and evaluation of the mechanical property. J Japan Soc Compos Mater 2011; 37:138-146. (in Japanese)

[3] Ishikawa T, Amaoka K, Masubuchi Y, Yamamoto T, Yamanaka A, Arai M, Takahashi J. Overview of automotive structural composites technology developments in Japan. Compos Sci Technol 2018; 155: 221-246.

[4] Taketa I, Okabe T, Kitano A. A new compression-molding approach using unidirectionally arrayed chopped strands. Compos Part A 2008; 39:1884–1890.

[5] Taketa I, Okabe T, Kitano A. Strength improvement in unidirectional arrayed chopped strands with interlaminar toughening. Compos Part A 2009; 40: 1174–1178.

[6] Taketa I, Sato N, Kitano A, Nishikawa M, Okabe T. Enhancement of strength and uniformity in unidirectionally arrayed chopped strands with angled slits. Compos Part A 2010; 41:1639–1646.

[7] Fujita Y, Matsutani H, Kawamoto S, Takehara T, Taketa I. Mechanical property and flowability of quasi-isotropic UACS laminates. Proc. 16th European Conference on Composite Materials, Seville, Spain, June 2014.

[8] Taketa I, Okabe T, Matsutani H, Kitano A. Flowability of unidirectionally arrayed chopped strands in compression molding. Compos Part B 2011; 42:1764–1769.

[9] Li H, Wang W-X, Takao Y, Matsubara T. New designs of unidirectionally arrayed chopped strands by introducing discontinuous angled slits into prepreg. Compos Part A 2013; 45:127–133.

[10] Sudarsono, Ogi K. Fatigue behavior of open-holed CFRP laminates with initially cut fibers. Open J Compos Mater 2017; 7: 49-62.

[11] Sudarsono, Ogi K. Effect of fiber cutting angle on the fatigue behavior of open-holed CFRP laminates with initially cut fibers. Materials System 2017; 35: 37-44.

[12] Li H, Wang W-X, Matsubara T. Multiscale analysis of damage progression in newly designed UACS laminates. Compos Part A 2014; 57: 108–117.

[13] Kravchenko SG, Sommer DE, Pipes RB. Uniaxial strength of a composite array of overlaid and aligned prepreg platelets. Compos Part A 2018; 109: 31-47.

[14] Kravchenko SG, Sommer DE, Denos BR, Avery WB, Pipes RB. Structure-property relationship for a prepreg platelet molded composite with engineered meso-morphology. Compos Struct 2019; 210: 430-445.

[15] Yashiro S, Ogi K. Fracture behavior in CFRP cross-ply laminates with initially cut fibers. Compos Part A 2009; 40: 938–947.

[16] Belytschko T, Black T. Elastic crack growth in finite elements with minimal remeshing. Int J Numer Meth Eng 1999; 45:601-620.

[17] Möes N, Dolbow J, Belytschko T. A finite element method for crack growth without remeshing. Int J Numer Meth Eng 1999; 46:131-150.

[18] Fries T-P, Belytschko T. The extended/generalized finite element method: An overview of the method and its applications. Int J Numer Meth Eng 2010; 84:253-304.

[19] Yashiro S, Takeda N, Okabe T, Sekine H. A new approach to predicting multiple damage states in composite laminates with embedded FBG sensors. Compos Sci Technol 2005; 65: 659–667.

[20] Geubelle PH, Baylor JS. Impact-induced delamination of composites: a 2D simulation.

Compos Part B 1998; 29:589–602.

[21] Kusaka T, Hojo M, Ochiai S, Kurokawa T. Rate-dependent mode II interlaminar fracture behavior of carbon-fiber/epoxy composite laminates. Materials Science Research International 1999; 5(2): 98-103.

[22] Ogihara S, Matuda K. Evaluation of mode III interlaminar fracture toughness of laminated composites. Proceedings of the 16th International Conference on Composite Materials (ICCM-16), Kyoto, 8-13 July 2007.

[23] Suemasu H. Analytical approaches to compression after impact (CAI) behavior of carbon fiber-reinforced composite materials. Adv Compos Mater 2016; 25:1-18.

[24] Owen DRJ, Hinton E. Finite elements in plasticity. Swansea: Pineridge Press; 1980.

[25] Yashiro S, Okabe T. Estimation of fatigue damage in holed composite laminates using an embedded FBG sensor. Compos Part A 2011; 42: 1962–1969.

[26] Yashiro S, Ogi K. Experimental study on shear-dominant fiber failure in CFRP laminates by out-of-plane shear loading. J Compos Mater 2019; 53: 1337–1346.

Figure captions

Figure 1 Typical layout of slits introduced in UACS laminates: (a) orthogonal discontinuous slits and (b) diagonal continuous slits.

Figure 2 Scanning electron microscope image of the delaminated surface of (a) the 0°/0° interface in a unidirectional UACS laminate and (b) the -45°/90° interface in a quasi-isotropic UACS laminate. The UACS laminates with 90° slit angle broke by delamination, and the point 1 mm apart from the slit was observed.

Figure 3 Layer-wise finite element model of a quasi-isotropic UACS laminate. The finite-element mesh with the exception of the top layer was omitted.

Figure 4 Layout of slits with an inclined angle of 27° from the fiber-direction that is shown by white arrows.

Figure 5 Predicted stress–strain curves of the UACS quasi-isotropic laminates.

Figure 6 Relationship between the tensile strength of the UACS quasi-isotropic laminates and slit angle. Supplementary experiment was conducted for comparison with the present analysis.

Figure 7 Distribution of the parameter *s* of cohesive elements indicating delamination growth in a UACS quasi-isotropic laminate with slit angle of 16°.

Table 1 Material properties used in the analysis.

(a) Mechanical properties of CFRP unidirectional lamina [4,6,25]

Longitudinal Young's modulus E_1 (GPa)	130
Transverse Young's modulus E_2 (GPa)	7.4
In-plane shear modulus G_{12} (GPa)	4.5
In-plane Poisson's ratio v_{12}	0.34

(b) Interlaminar shear properties [4,26]

Mode II critical energy release rate G_{IIc} (J/m^2)	633
Mode III critical energy release rate G_{IIIc} (J/m^2)	633
In-plane shear strength $\tau_{t\,max}$ (MPa)	60
Out-of-plane shear strength $\tau_{b\,max}$ (MPa)	60

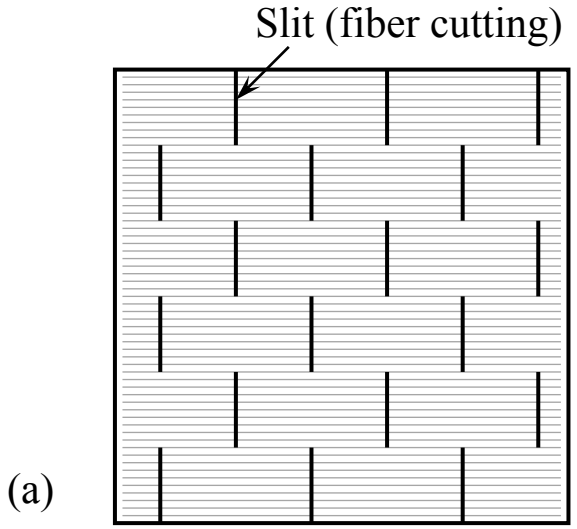

(a)

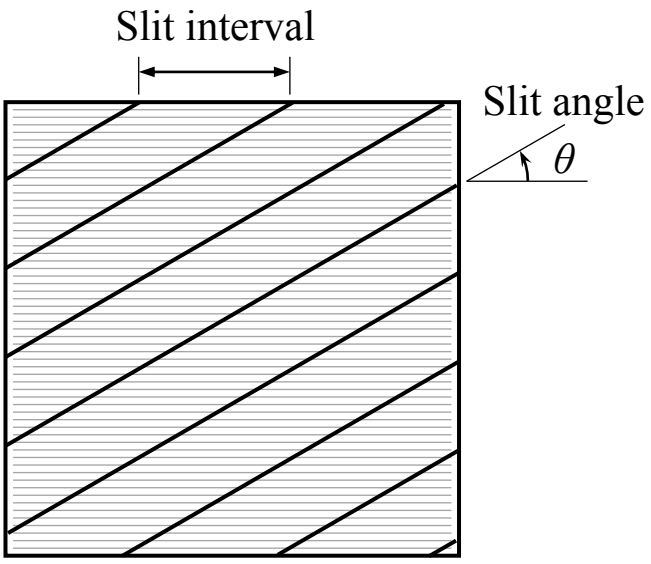

(b)

Figure 1

(a)

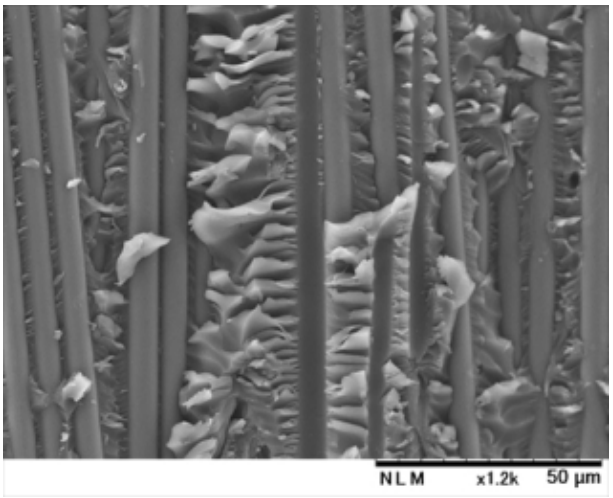

(b)

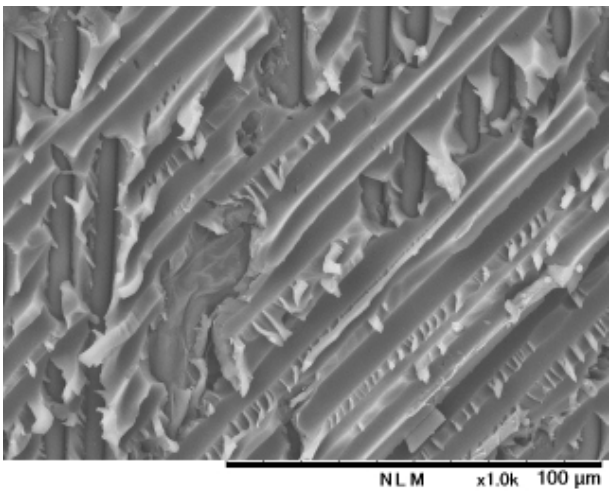

Figure 2

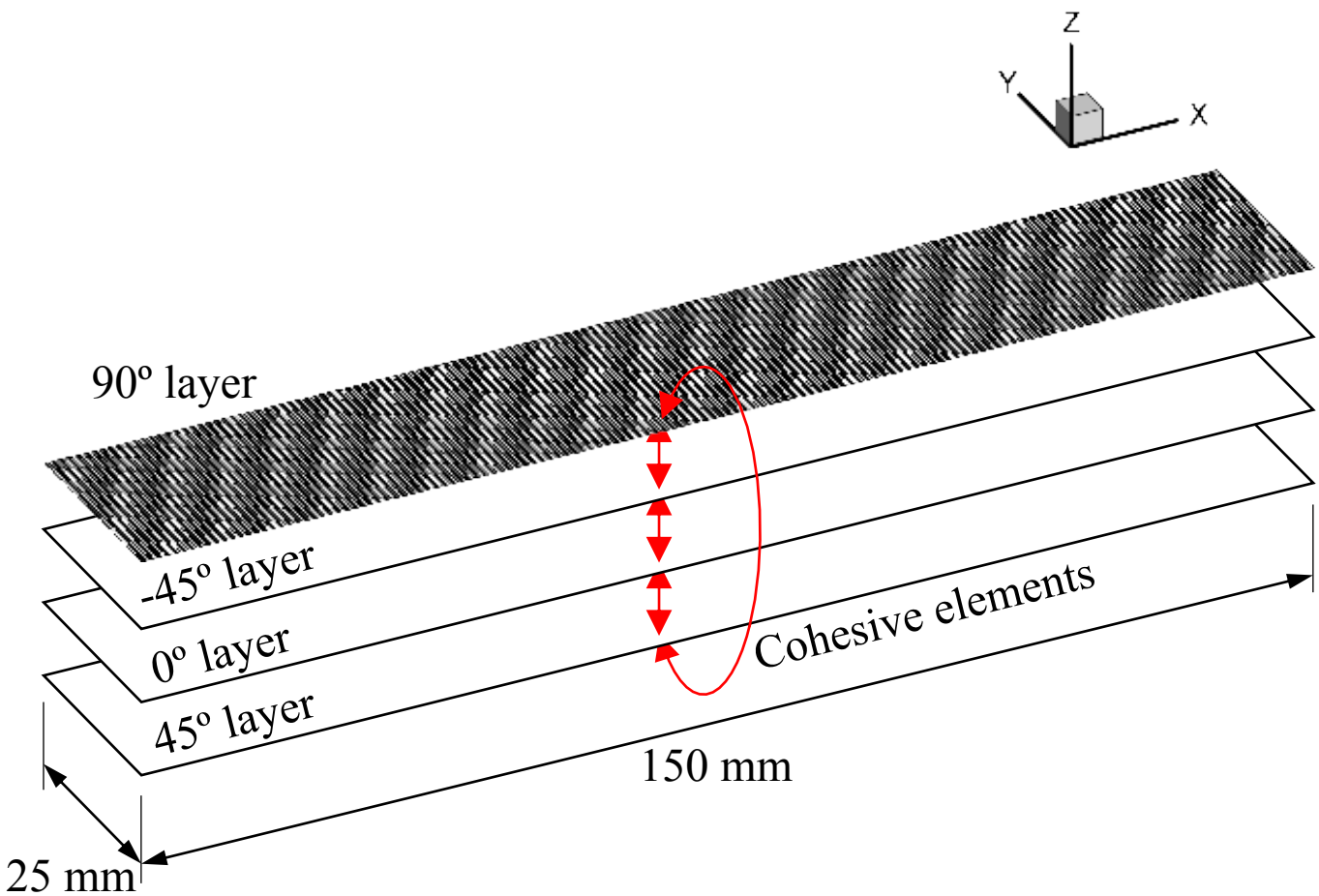
Z
Y
X
90º layer
-45º layer
0º layer
45º layer
Cohesive elements
150 mm
25 mm

Figure 3

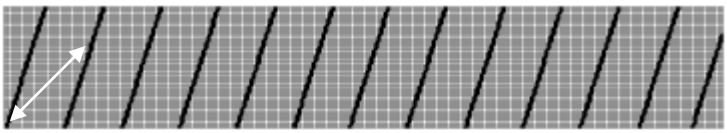

(a) 45º layer

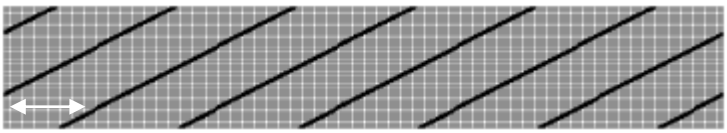

(b) 0º layer

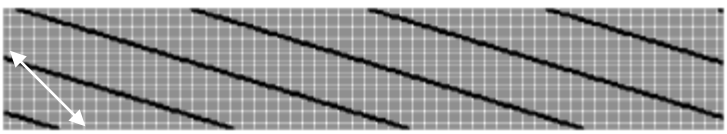

(c) -45º layer

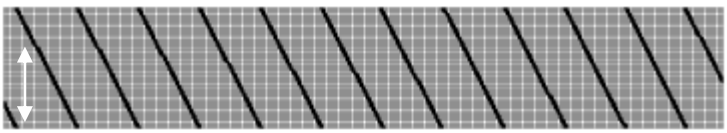

(d) 90º layer

Figure 4

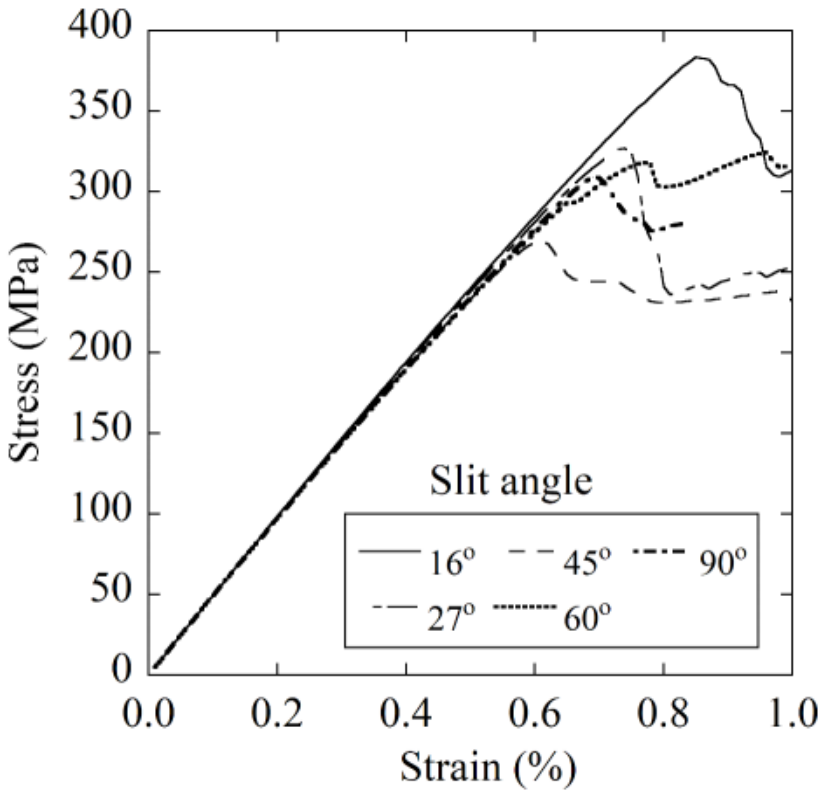
400
350
300
250
200
150
100
50
0
Stress (MPa)
0.0
0.2
0.4
0.6
0.8
1.0
Strain (%)
Slit angle
16°
45°
90°
27°
60°

Figure 5

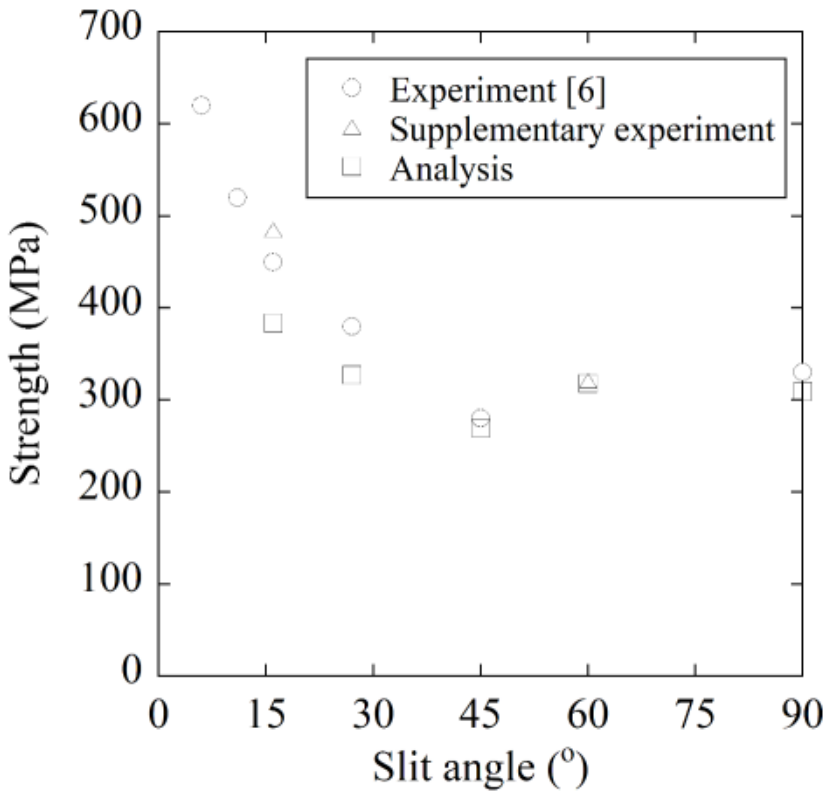
Experiment [6]
Supplementary experiment
Analysis
Strength (MPa)
Slit angle (°)
0
100
200
300
400
500
600
700
0
15
30
45
60
75
90

Figure 6

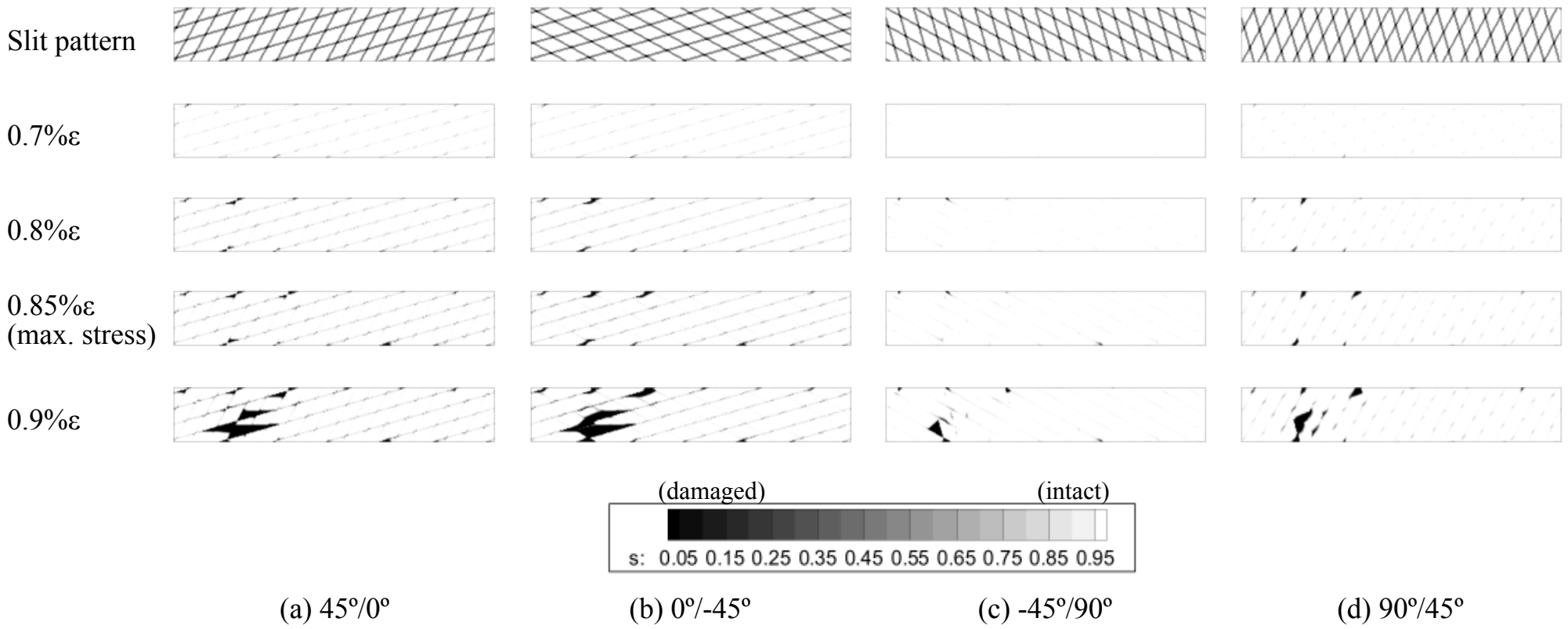
Slit pattern
0.7%ε
0.8%ε
0.85%ε
(max. stress)
0.9%ε
(damaged)
(intact)
s: 0.05 0.15 0.25 0.35 0.45 0.55 0.65 0.75 0.85 0.95
(a) 45º/0º
(b) 0º/-45º
(c) -45º/90º
(d) 90º/45º

Figure 7

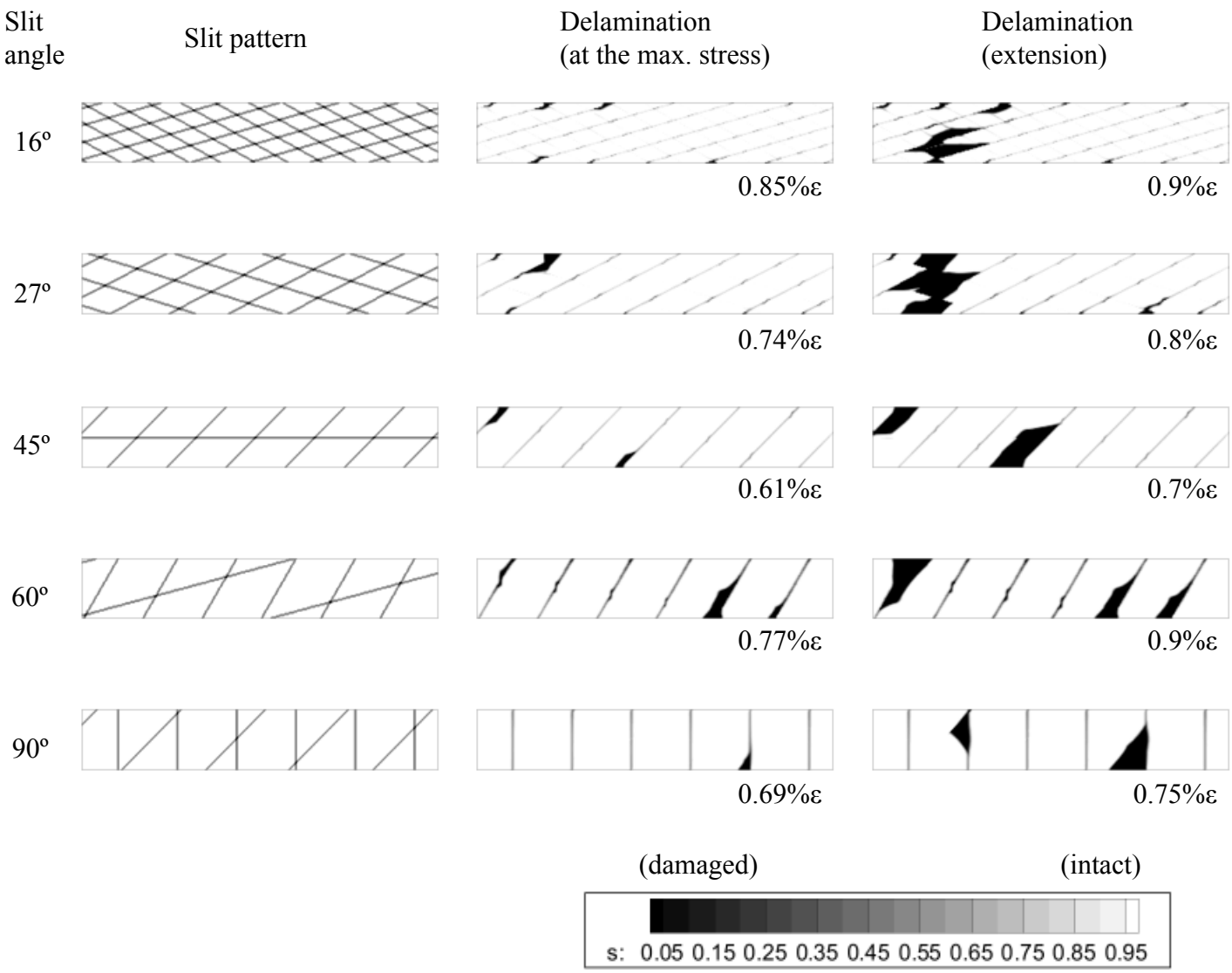
Slit angle
Slit pattern
Delamination (at the max. stress)
Delamination (extension)
16º
0.85%ε
0.9%ε
27º
0.74%ε
0.8%ε
45º
0.61%ε
0.7%ε
60º
0.77%ε
0.9%ε
90º
0.69%ε
0.75%ε
(damaged)
(intact)
s: 0.05 0.15 0.25 0.35 0.45 0.55 0.65 0.75 0.85 0.95

Figure 8

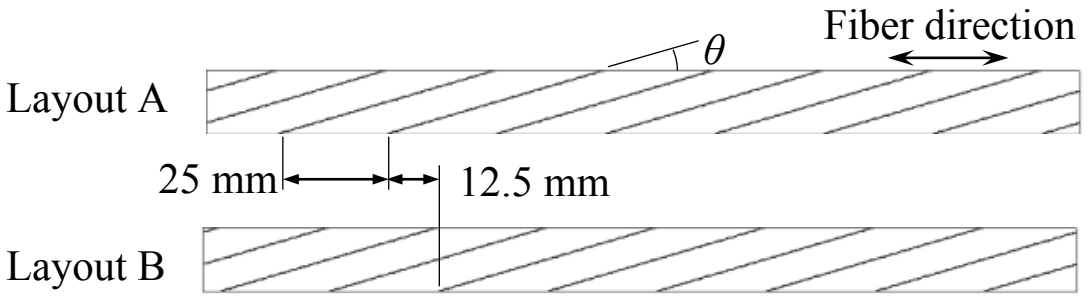

(a) Layout of slits

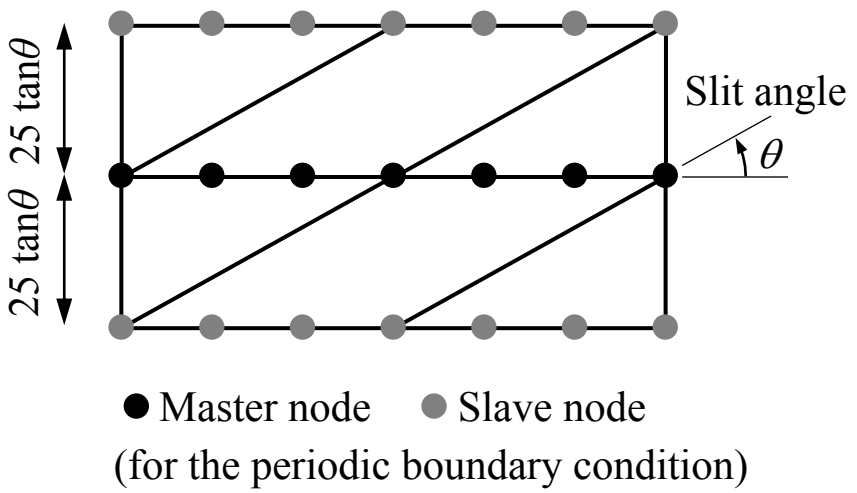

(b) Periodic structure in the transverse direction

Figure 9

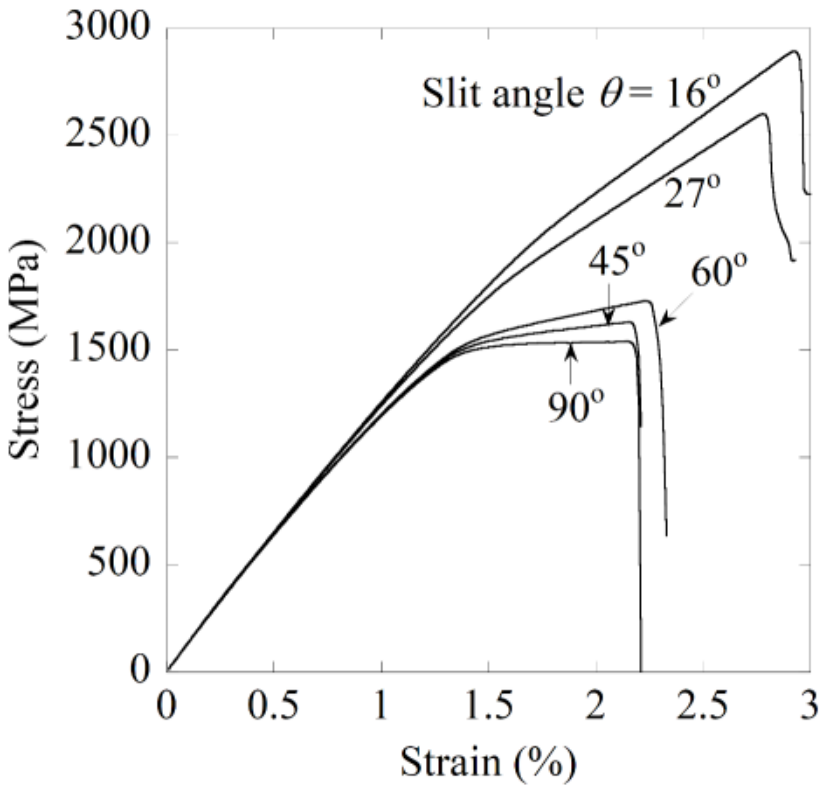
3000
2500
2000
1500
1000
500
0
Stress (MPa)
0
0.5
1
1.5
2
2.5
3
Strain (%)
Slit angle θ = 16°
27°
45°
60°
90°

Figure 10

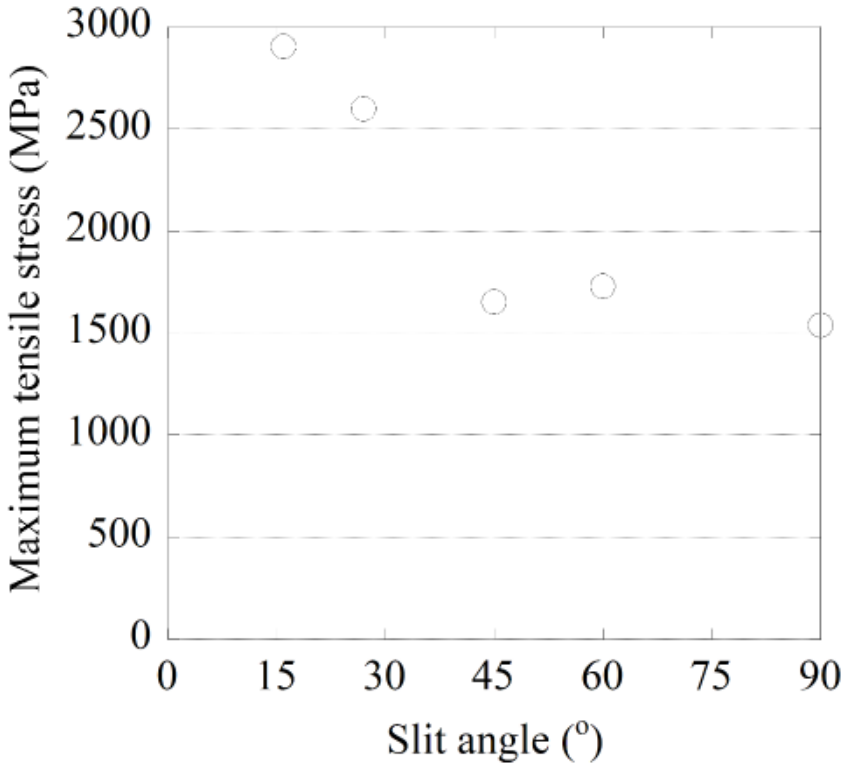
Maximum tensile stress (MPa)
3000
2500
2000
1500
1000
500
0
0
15
30
45
60
75
90
Slit angle (°)

Figure 11

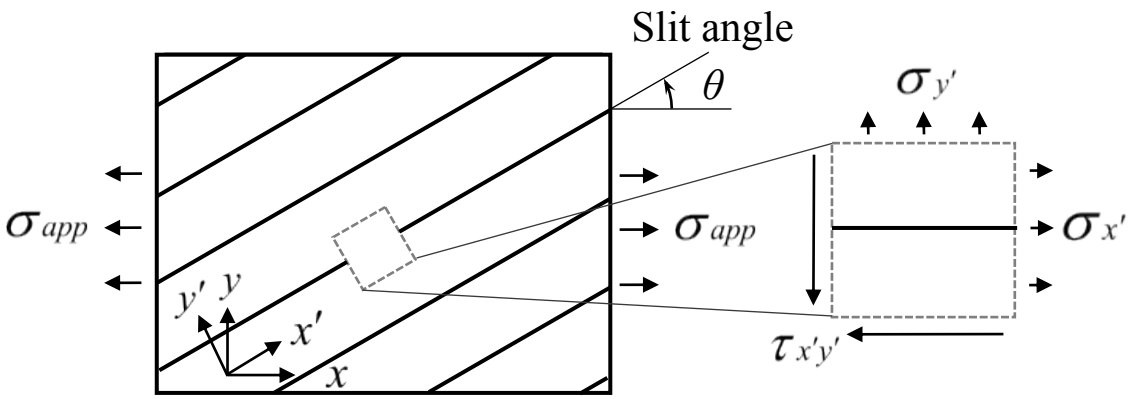

Figure 12

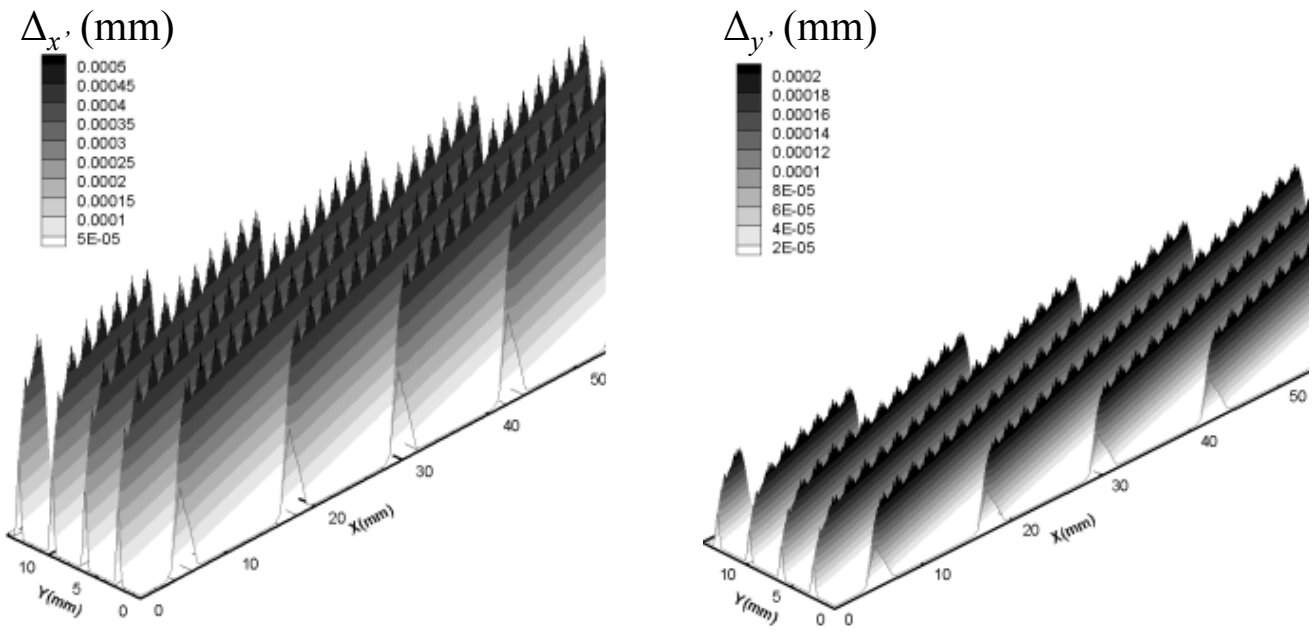

(a) $\theta = 16^{\circ}$

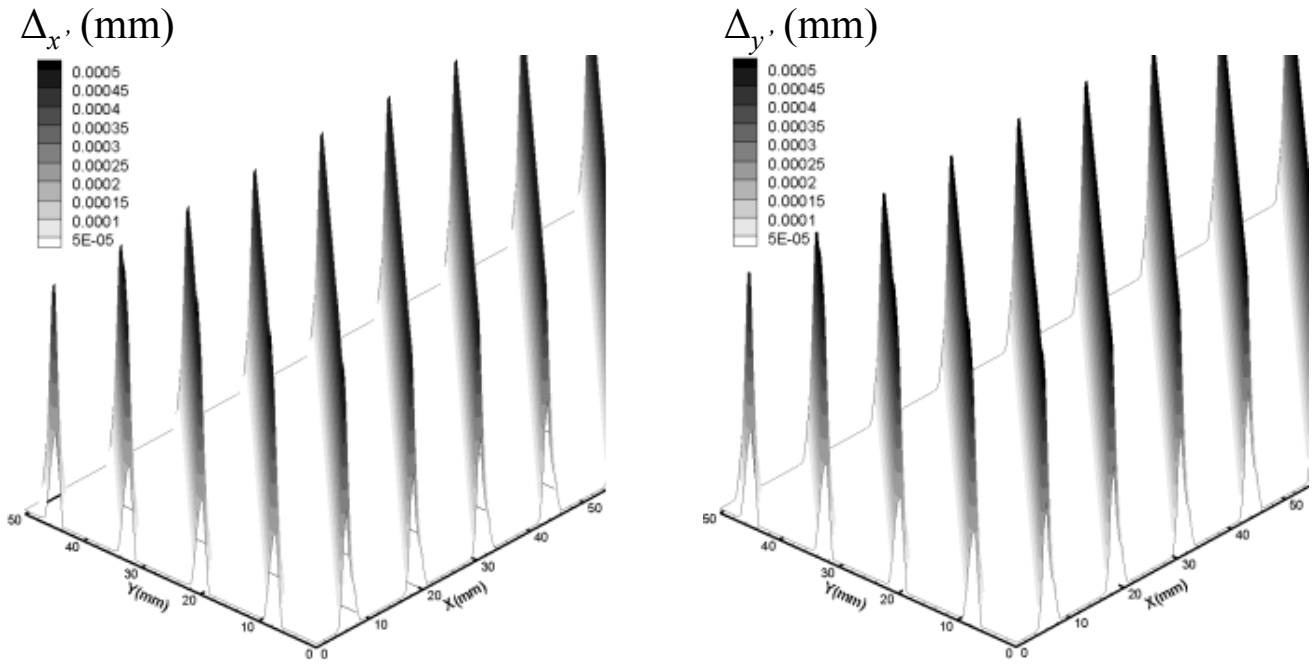

(b) $\theta = 45^{\circ}$

Figure 13